Received: 23 December 2016 | Revised: 1 March 2017 | Accepted: 4 March 2017
DOI: 10.1002/aoc.3818

FULL PAPER

WILEY Applied Organometallic Chemistry

Syntheses, structures and catecholase activities of homo- and hetero-trinuclear cobalt(II) complexes constructed from an acyclic naphthalenediol-based bis(Salamo)-type ligand

Li-Hong Li | Wen-Kui Dong | Yang Zhang | Sunday Folaranmi Akogun | Li Xu

School of Chemical and Biological Engineering, Lanzhou Jiaotong University, Lanzhou 730070, China

Correspondence
Wen-Kui Dong, School of Chemical and Biological Engineering, Lanzhou Jiaotong University, Lanzhou 730070, China.
Email: dongwk@126.com

Funding Information
National Natural Science Foundation of China, Grant/Award Number: 21361015

A series of homo- and hetero-trinuclear cobalt(II) complexes $[Co_3(L)(OAc)_2(CH_3CH_2OH)(H_2O)]$ (**1**), $[Co_2Ba(L)(OAc)_2]$ (**2**) and $[Co_2Ca(L)(OAc)_2]\cdot CHCl_3$ (**3**), containing an acyclic naphthalenediol-based ligand H_4L were synthesized. All the three complexes were characterized by elemental analyses, IR, UV–vis spectra and single crystal X-ray diffraction analyses. Comparative studies of the structures and spectroscopic properties are carried out on these complexes. All of the complexes show catechol oxidase activities in MeCN. Using UV–vis spectroscopy, we monitored the aerial oxidation of 3,5-di-*tert*-butylcatechol (3,5-DTBCH$_2$) to 3,5-di-*tert*-butylquinone (3,5-DTBQ), which confirms the essential role of these complexes in enhancing the catalytic reaction.

KEYWORDS
acyclic naphthalenediol-based ligand, catalysis, crystal structure, trinuclear cobalt(II) complex, UV–vis titration

1 | INTRODUCTION

The coordination chemistry of transition metal complexes with Salen-type N_2O_2 tetradentate ligands (N,N′-disalicylideneethylenediamine) have achieved a considerable attention in the past decades due to their potential application in catalysts,[1] biological fields,[2–6] electrochemical conducts,[7] nonlinear optical materials,[8] magnetic materials,[9] luminescence properties[10–13] and supramolecular architecture.[14–20] Chemical modifications of substituent or functional groups in the Salen N_2O_2 ligands are effective in exchanging the structures or the main functions of the complexes, such as Salamo ligand, a Salen's analogue, (R-CH = N-O-(CH)$_n$-O-N = CH-R) is one of the most versatile ligand.[15,21–30] Noticeably, a number of works have been devoted to synthesize and characterize mono-, di- and multinuclear transition metal(II) complexes bearing mono (Salamo)-type ligand orits derivatives.[31–44] An acyclic bis (Salamo)-type ligand H_4L exists in which two Salamo chelate moieties share one benzenediol ring. When the two Salamo moieties coordinate with d-block transition metals, the conformation of the molecules is restricted so that the phenoxo oxygen atoms are directed inward to form an O_6 cavity, which can coordinate through the negatively charged phenoxo groups to metal atoms, but there are relatively few researches on bis(Salamo) ligands and their complexes.[24]

As important raw materials and intermediates in organic chemical, catechins have a wide range of applications in agriculture, pharmaceutical, photographic materials and other fields.[45] In this paper, we have designed and synthesized a naphthalenediol-based acyclic symmetric bis(Salamo)-type tetraoxime ligand in which two Salamo chelate moieties share one naphthalenediol ring, and reported the syntheses and characterizations of three new homo- and hetero-trinuclear cobalt(II) complexes, $[Co_3(L)(OAc)_2(CH_3CH_2OH)(H_2O)]$ (**1**), $[Co_2Ba(L)(OAc)_2]$ (**2**) and $[Co_2Ca(L)(OAc)_2]\cdot CHCl_3$ (**3**), and then studied their catechol oxidase activities. The experimental results show that those Co(II) complexes have good catalytic activities, and act as enzyme in the catalysis of catechol to quinone.

2 | RESULTS AND DISCUSSION

2.1 | Synthesis of complexes 1, 2 and 3

The three homo- and hetero-trinuclear cobalt(II) complexes **1**, **2** and **3** were prepared by the reaction of the ligand (H_4L) with $Co(OAc)_2{\cdot}4H_2O$ in 1:3 molar ratio (for **1**), the ligand (H_4L) with $Co(OAc)_2{\cdot}4H_2O$ and $Ba(OAc)_2$ in 1:2:1 ratio (for **2**) and the ligand (H_4L) with $Co(OAc)_2{\cdot}4H_2O$ and $Ca(OAc)_2{\cdot}H_2O$ in 1:2:1 ratio (for **3**), respectively. It's worth noting that the coordination mode of the center metal(II) atom in homo-trinuclear complex **1** is different from hetero-trinuclear complexes **2** and **3**. Practically, alkaline earth metal(II) (Ba(II) and Ca(II)) atoms are more likely to occupy the ligand O_6 cavity relative to transition metal(II) (Co(II)) atom, thus, the Co(II) atoms are easily to be replaced, and eventually form a series of hetero-trinuclear complexes. This may be due to O_6 cavity that is bigger than N_2O_2 cavity, and being in the same period, the radius of the alkaline earth metal atoms is larger than the transition metal atoms, therefore, Ba(II) and Ca(II) atoms could easily fit into the O_6 cavity than alkaline earth metal(II) atoms.

2.2 | Description of the structures of complexes 1, 2 and 3

Structural analyses reveal the existence of various coordination modes of the Co(II) complexes. For instance, in homo-trinuclear complex **1**, the two terminal Co(II) atoms (Co1 and Co3) are penta-coordinated, nevertheless, the central Co(II) atom (Co2) is hexa-coordinated. In the same manner, for hetero-trinuclear complexes **2** and **3**, the coordination mode of the terminal Co(II) atoms (Co2 and Co3 for complex **2**, and Co1 and Co2 for complex **3**) is the same as homo-trinuclear complex **1**. The three metal(II) atoms are bridged by two chelating *μ*-acetate ions. The differences of the crystal structures in the three complexes are that the central metal(II) atoms having two type of coordination modes, and whether coordinating to the solvent molecules or 3-position ethyloxy group. The selected bond lengths and angles of the homo- and hetero-trinuclear complexes **1**, **2** and **3** are listed in Table S1.

2.2.1 | Crystal structure of $[Co_3(L)(OAc)_2(CH_3CH_2OH)(H_2O)]$ (1)

X-ray crystallographic analysis of complex **1** reveals the formation of a 1:3 ($(L)^{4-}$: Co(II)) trinuclear structure which is similar to the structure of reported earlier on the bis(Salamo)-type Co(II) complex, $[Co_3(6,6'\text{-diMeObisSalamo})(OAc)_2(CH_3CH_2OH)_2]{\cdot}2CHCl_3$.[26] Complex **1** crystallizes in the monoclinic system, space group $P2_1/n$ with three Co(II) atoms located at the three coordination environments of the $(L)^{4-}$ unit. From the thermal ellipsoid plot of **1**, it appears that the two terminal Co(II) centres (Co1 and Co3) of the trinuclear structure take different geometries from that of the central Co(II) atom (Co2) (Figure 1). The two *μ*-acetate groups bridged the three Co(II) atoms; Co1 and Co3 atoms are both penta-coordinated with distorted trigonal bipyramidal geometries, with estimated trigonality index (τ) values of 0.70 and 0.76 for Co1 and Co3 atoms, respectively.[44] Co2 atom is hexa-coordinated with a distorted octahedral geometry. In addition to the phenoxyl and *μ*-acetate oxygen atoms, two oxygen atoms from the coordinated water and ethanol molecules participate in the coordination, thus, the geometries reflecting the

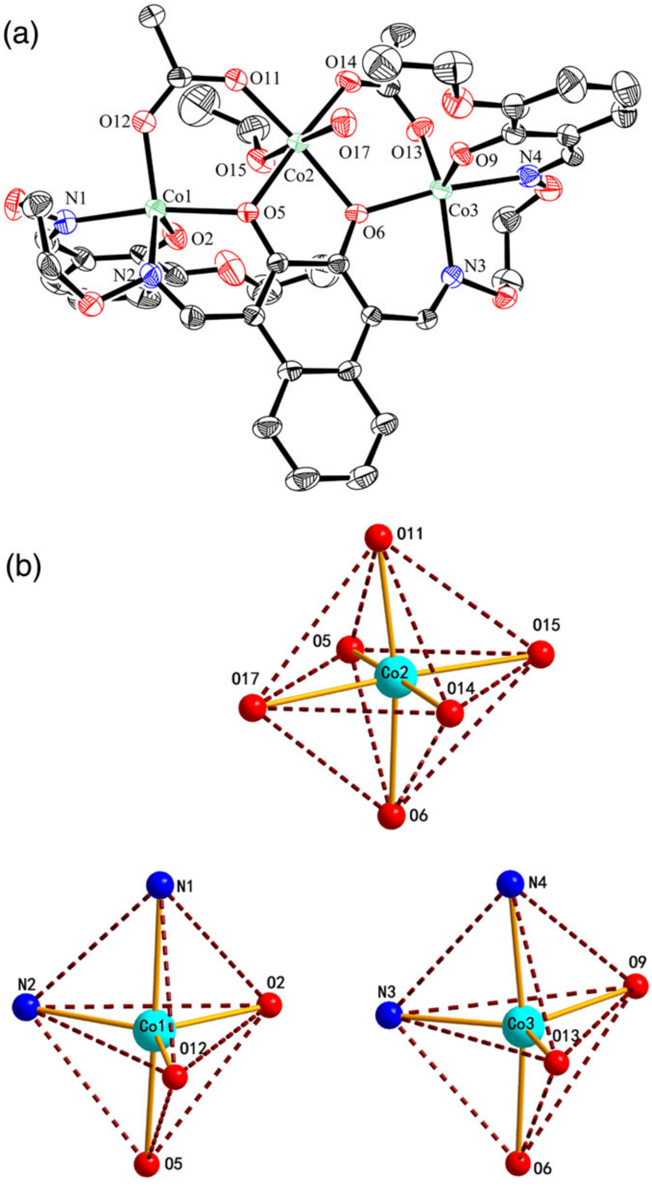

FIGURE 1 (a) molecule structure and atom numberings of complex **1** (hydrogen atoms are omitted for clarity and thermal ellipsoids are drawn at the 30% probability level.). (b) coordination polyhedra for Co(II) atoms of complex **1**

coordination environment of Co(II) atoms in **1** is also shown in Figure 1. The distances between Co2 atom and the six coordinated oxygen atoms are between 2.020(4) and 2.140 (3) Å, and the coordinate bond lengths between Co1 and Co3 atoms and the coordinated atoms are in the range of 1.923(4) and 2.113(4) Å. Interestingly, the terminal benzene rings of the Co(II) complexes $[Co_3(L)(OAc)_2(CH_3CH_2OH)(H_2O)]$ are bent toward the same side and the dihedral angles of naphthalene and the two benzene rings are 83.17(4)°(for C3-C8) and 84.55(4)°(for C27-C32), respectively. The same phenomenon also appears in the case of the cobalt(II) complex, $[Co_3(6,6'\text{-diMeObisSalamo})(OAc)_2(CH_3CH_2OH)_2]\cdot 2CHCl_3$.[26] The two μ-acetate groups are on the same side of the plane which contains the two benzene rings, and the dihedral angle of the two μ-acetate groups is 42.24(3)°.

There are intramolecular and intermolecular hydrogen bonds in complex **1**. The parameter values of the hydrogen bonds in **1** are listed in Table S2. The intramolecular hydrogen bonds in **1** are depicted in Figure 2. Finally, **1** forms an infinite1D supramolecular structure by C–H···π (C11′–H11D···Cg9) interactions of neighboring complex **1** molecules as shown in Figure 3.[29,33,44]

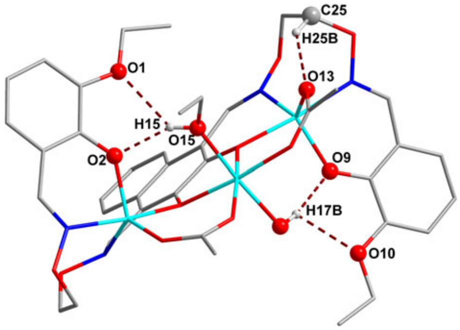

FIGURE 2 Intramolecular hydrogen bonding interactions of complex **1**

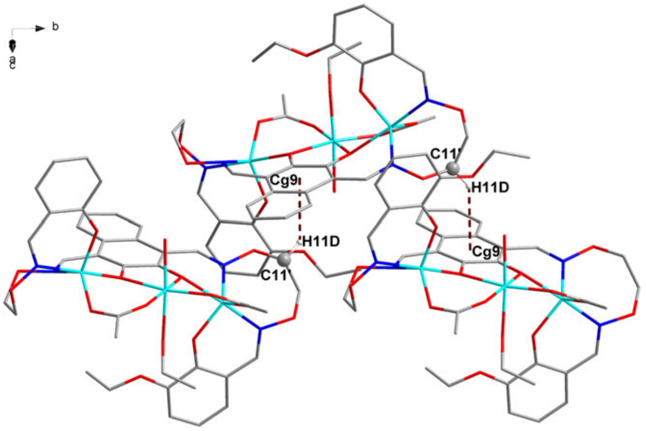

FIGURE 3 C–H···π interactions of complex **1**

2.2.2 | Crystal structure of $[Co_2Ba(L)(OAc)_2]$ (2)

Complex **2** crystallizes in the triclinic, space group *P*-1. The two Co(II) atoms (Co2 and Co3) are located at the N_2O_2 cavities, and Ba(II) atom occupied O_6 cavity, with the two μ-acetate ions bridging the three metal(II) atoms. Calculated values of τ were found to be 0.46 and 0.27 for Co2 and Co3, respectively.[46] Therefore, penta-coordinated Co2 atom and its geometry is roughly between trigonal bipyramid and square pyramid; Co3 atom is penta-coordinated with a distorted square pyramid geometry. Interestingly, the coordination pattern of the center metal(II) atom Ba(II)

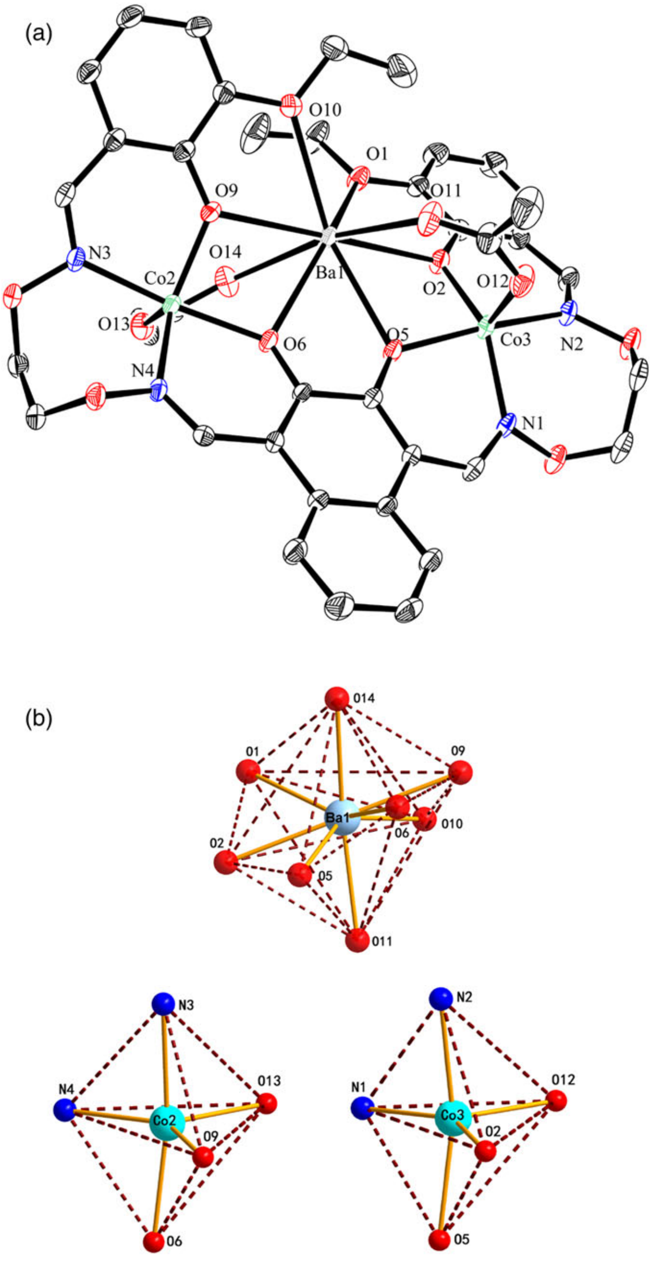

FIGURE 4 (a) molecule structure and atom numberings of complex **2** (hydrogen atoms are omitted for clarity and thermal ellipsoids are drawn at the 30% probability level.). (b) coordination polyhedra for Co(II) and Ba(II) atoms of complex **2**

is different from complex **1**, where both ethoxy oxygen atoms (O1 and O10) are involved in the coordination, forming a octa-coordinated trihedral dodecahedron geometry. Molecular structure and coordination environment of complex **2** are drawn in Figure 4. The distances between Ba1 and the four phenoxy oxygen atoms (O2, O5, O6 and O9) of the $(L)^{4-}$ units are in range of 2.658(2) and 2.745(2) Å, which are obviously shorter than the ethoxy groups (Ba1-O1 2.873(2) Å, Ba1-O10 2.862(3) Å), and the coordinate bond lengths between Co2 and Co3 atoms and the coordinated atoms are in the range of 1.979(2) and 2.116(2) Å, which is close to the length of coordinate bonds between Co1 and Co3 atoms and the coordinated atoms of complex **1**. The terminal benzene rings of complex **2** are located at both sides and the angles between the plane of naphthalene ring and the plane of two benzene rings are range from 8.99(3)° (C27-C31) to 41.28(4)° (C3-C8). The two bridged *μ*-acetate ions are located on both sides of the plane of the naphthalene ring, and the dihedral angle is 61.27(3)°.

The parameter values of the hydrogen bonds in **2** are listed in Table S2. The intramolecular hydrogen bonds in complex **2** are shown in Figure S1. In the crystal structure of complex **2**, there are significant intermolecular hydrogen bonds (C18-H18···O8), which links complex **2** molecules together efficiently.[35,44] Figure 5 shows an infinite 1D supramolecular structure along the certain axis.

2.2.3 | Crystal structure of $[Co_2Ca(L)(OAc)_2]\cdot CHCl_3$ (3)

Complex **3** crystallizes in the triclinic, space group *P*-1 with the two Co(II) atoms (Co1 and Co2) located at the N_2O_2 cavities and Ca1 atom occupied O_6 cavity, and two *μ*-acetate ions bridged the three metal(II) atoms. The coordination mode of terminal Co(II) atoms is the same as complex **2**. The two *μ*-acetate ions bridged the three metal(II) atoms. Co1 and Co2 atoms are both penta-coordinated with distorted square pyramid geometries having trigonality index values (τ) estimated to be 0.28 and 0.16 for Co1 and Co2 atoms,[46] respectively. Similarly, just as in **2**, phenoxy oxygen atoms (O1, O2, O5 and O7) of the $(L)^{4-}$ units, two *μ*-acetate oxygen atoms (O10 and O14) and both ethoxy oxygen atoms (O6 and O12) are involved in coordination, the central Ca(II) atom is octa-coordinated and has a distorted square antiprism. Therefore, the coordination pattern of the central Ca(II) atom is different from that of the central Co2 atom in complex **1**. Complex **3** and its coordination environment are shown in Figure 6. The distances between Ca1 atom and the four phenoxy oxygen atoms of the $(L)^{4-}$ units are ranged from 2.388(3) to 2.423(3) Å, which are obviously shorter than the ethoxy groups (Ca1-O6 2.631(4) Å, Ca1-O12 2.664(4) Å), and the coordinate bond lengths between Co1 and Co2 atoms and the coordinated atoms are in the range of 1.983 (3) and 2.077(4) Å, which is close to the length of coordinate bonds between Co1 and Co3 atoms and the coordinated atoms of complex **1**. The terminal benzene rings of complex **3** are located at both sides and the angles between the plane of naphthalene ring and the planes of two benzene rings are range from 7.58(3)° (C29-C34) to 42.06(4)° (C16-C21). The two bridged *μ*-acetate ions are located at both sides of the plane of the naphthalene ring, and the dihedral angle is 52.12(4)°.

The parameter values of the hydrogen bonds in **3** are listed in Table S2. The intramolecular hydrogen bonds in complex **3** are shown in Figure S2. In the crystal structure of complex **3**, there are significant intermolecular hydrogen bonds (C4–H4···O4 and C23–H23···O4), which links complex **3** molecules together efficiently. [34,44] Figure 7 shows an infinite 1D supramolecular structure along the certain axis. It is worth noting that in complex **3**, a dimer is formed via hydrogen bonding interactions, just as shown in Figure 8.

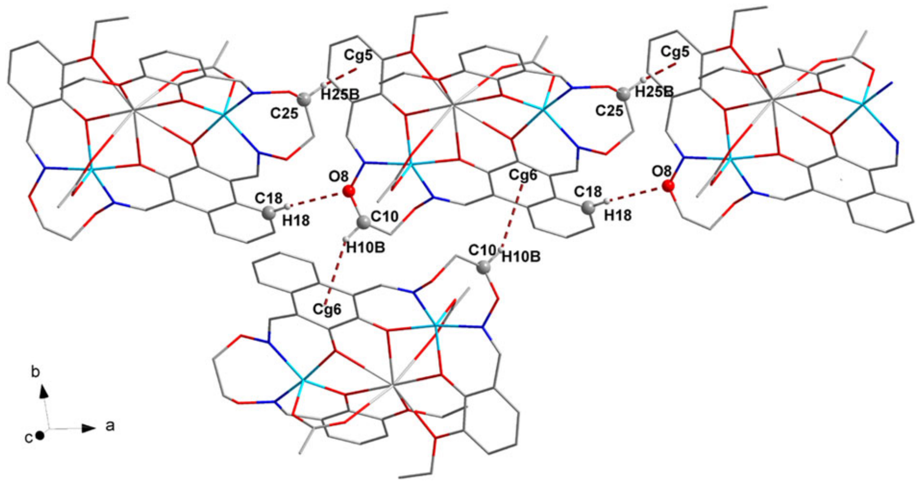

FIGURE 5 View of the 2D motif for complex **2**

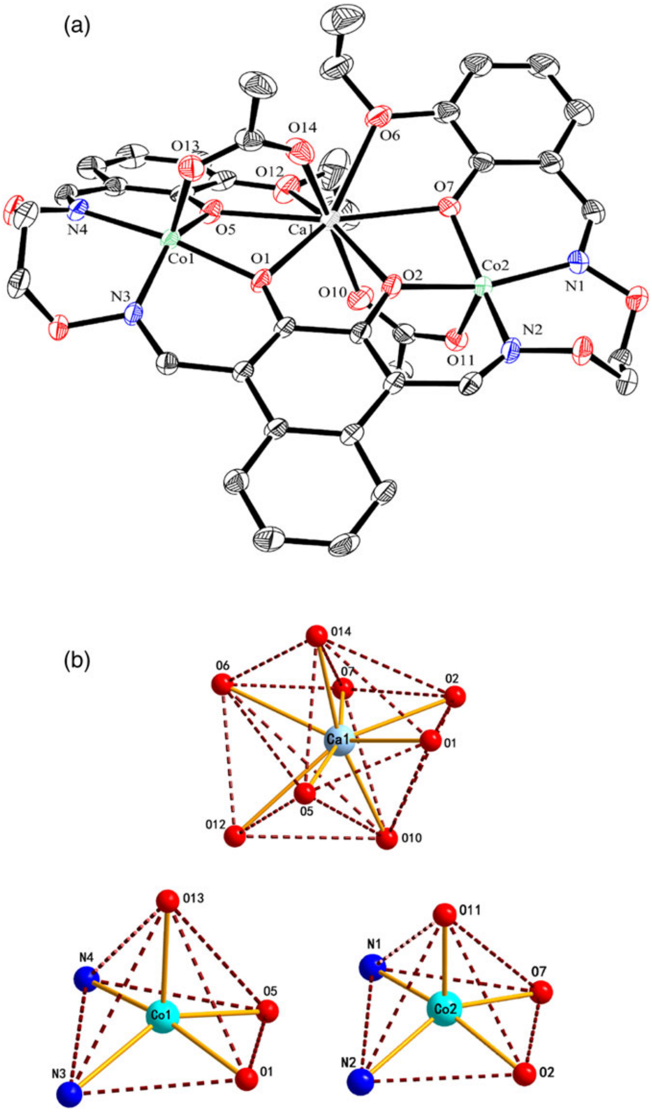

FIGURE 6 (a) molecule structure and atom numberings of complex **3** (hydrogen atoms and solvent molecule are omitted for clarity and thermal ellipsoids are drawn at the 30% probability level). (b) coordination polyhedra for Co(II) and Ca(II) atoms of complex **3**

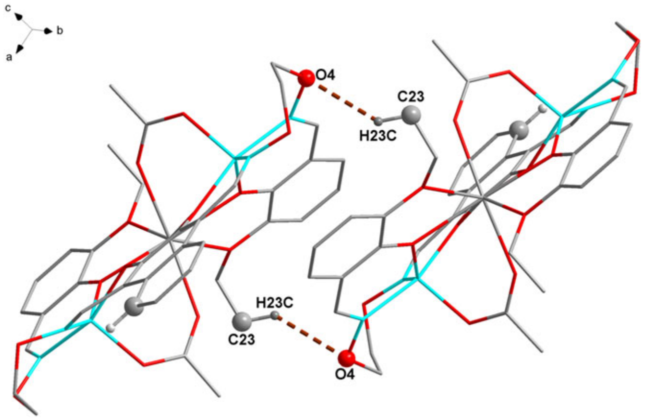

FIGURE 8 View of a dimer of complex **3** formed by hydrogen bonds

2.3 | IR and UV–vis spectra of complexes 1, 2 and 3

The IR spectrum of ligand H_4L contains characteristic band of C = N stretching vibrations at 1605 cm^{-1}, which is shifted to 1592, 1585 and 1590 cm^{-1} in the spectra of complexes **1**, **2** and **3**, respectively, which indicating that the nitrogen atoms of C = N group are coordinated to the metal(II) atoms.[31,34]

The Ar–O stretching vibration band of ligand H_4L is observed at 1257 cm^{-1}, while these bands appear at 1205, 1210 and 1206 cm^{-1} in the spectra of the metal(II) complexes, respectively. The Ar–O stretching frequencies shifted to a lower frequencies, indicating that the M–O bonds are formed between the metal(II) atoms and oxygen atoms of phenolic groups.[32–37] In addition, the O–H stretching frequency of Salamo-type ligands is usually observed at 3300–3500 cm^{-1} region, however, this frequency is generally shifted to *ca*. 3430 cm^{-1} due to the internal hydrogen bond OH···N = C. As the hydrogen bond becomes stronger, the bandwidth increases, and this band sometimes is not detected. Electron-donating groups on the phenolic ring increase the electron density on the hydroxyl oxygen making the H–O bond stronger, the absorption usually appears as a broad band in the FT-IR spectrum. Here, the O–H stretching band of ligand H_4L appears at 3391 cm^{-1}. These bands are

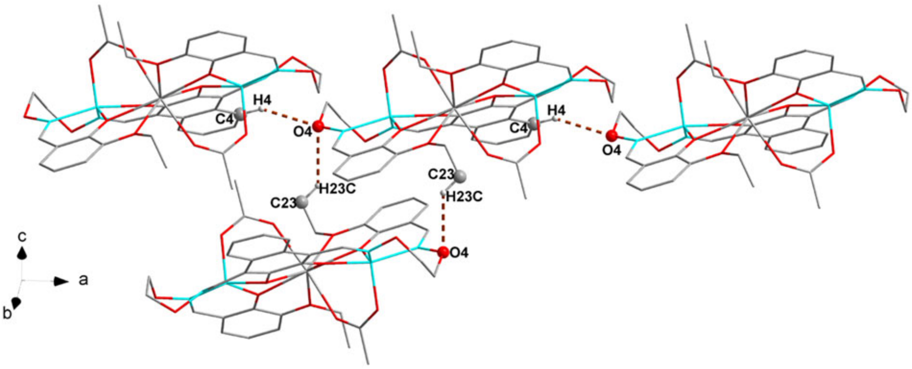

FIGURE 7 View of an infinite 1D chain motif of complex **3** units along the certain axis

weakened or disappeared in the IR spectra of complexes **1**, **2** and **3**, which is indicative of the fact that the phenolic OH groups of ligand H_4L have been deprotonized and coordinated to the metal(II) atoms.[31–34,43,44] The absorption band at 3429 cm^{-1} in complex **1** is assigned to the coordinated

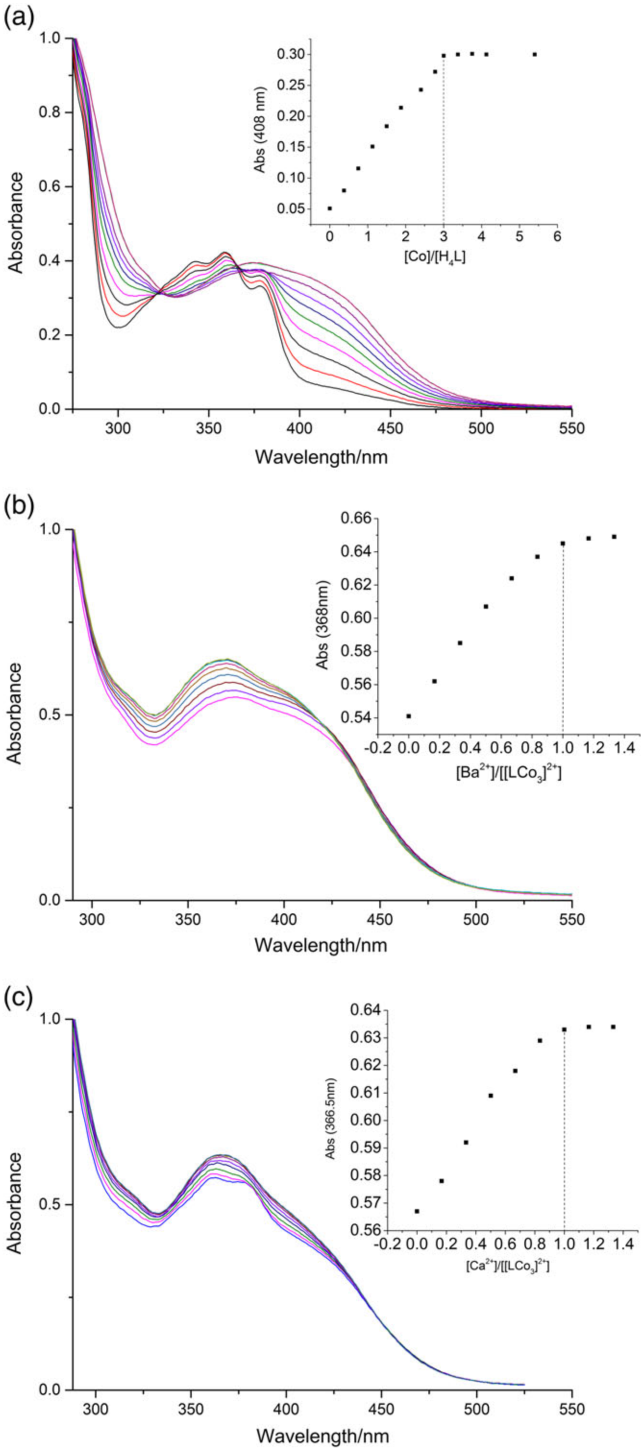

FIGURE 9 (a) UV–vis spectra changes of H_4L (2.5×10^{-5} M)upon addition of $Co(OAc)_2{\cdot}4H_2O$ (1.0×10^{-3} M), ($CHCl_3/CH_3OH$ (3:2). (b) UV–vis spectra changes of L-Co(II) complex upon addition of $Ba(OAc)_2$. (c) UV–vis spectra changes of L-Co(II) complex upon addition of $Ca(OAc)_2{\cdot}H_2O$

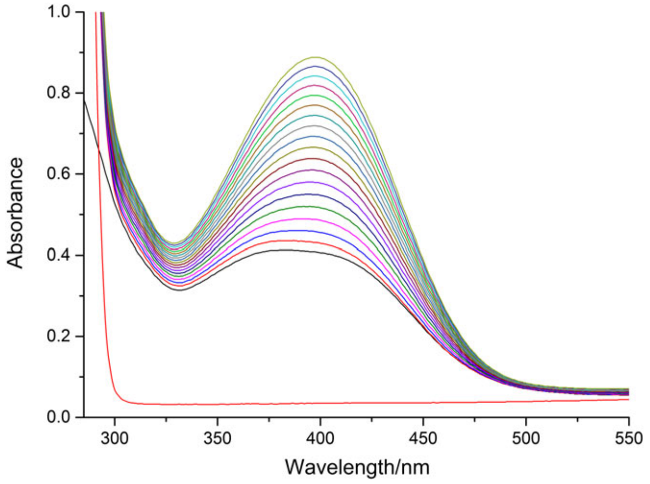

FIGURE 10 Increase of the quinone band at around 405 nm after the addition of 100 equivalents of 3,5-$DTBCH_2$ to MeCN solution with complex **1**. The spectra were recorded at 5 min intervals

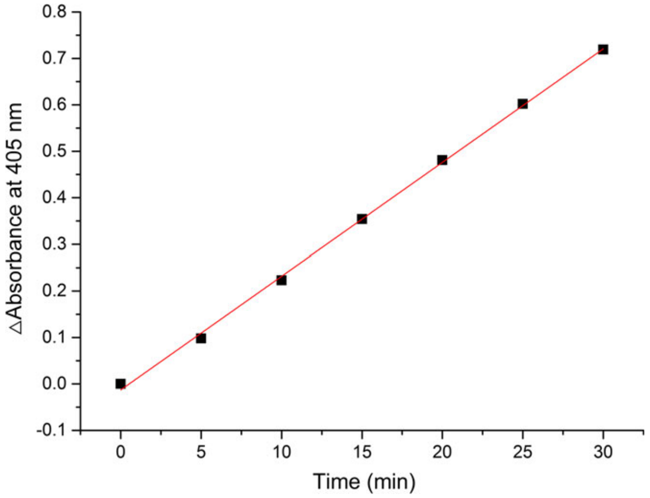

FIGURE 11 Plot of the difference in absorbance (ΔA) *vs*. time at 405 nm to evaluate the initial rate of the catalytic oxidation of 3,5-$DTBCH_2$ by complex **1** in MeCN

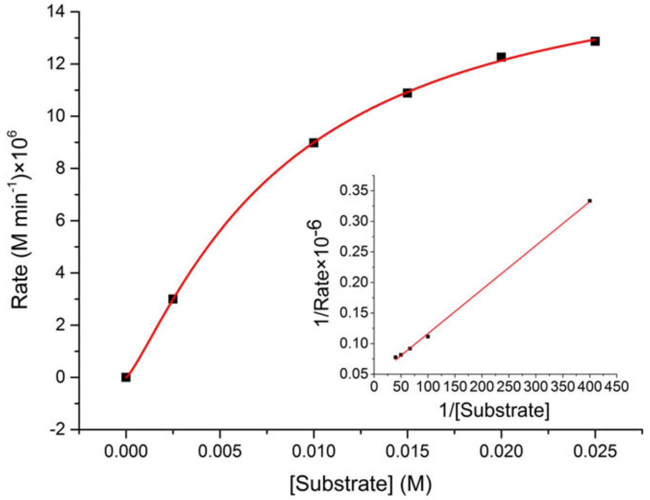

FIGURE 12 Plot of the rate *vs*. substrate concentration for complex **1**. The inset shows the corresponding Lineweaver-Burk plot

ethanol and water molecules which are confirmed by the crystal structure (Figure S3).

The UV–vis spectrum of ligand H_4L (2.5×10^{-5} M) was measured in $CHCl_3$:CH_3OH (3:2) solutions. In order to determine the reaction stoichiometry of ligand H_4L with the metal(II) atoms, UV–vis titration experiments were carried out on these complexes. The free ligand H_4L shows three strong absorption bands at 342, 359 and 378 nm.[36–38,44] In the case of complex **1**, the gradual addition of Co(II) ions brought changes to the absorption peaks, and addition up to 3 equiv resulted to one band at 374 nm which could be as

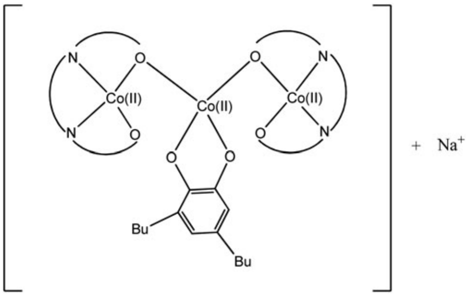

SCHEME 1 The plausible intermediate $[Co_3(L)(3,5\text{-DTBC})\text{-}Na]^+$ formed during the catecholase reaction

TABLE 1 Crystallographic data and refinement parameters for complexes **1**, **2** and **3**

Complex	1	2	3
Empirical formula	$C_{40}H_{45}Co_3N_4O_{16}$	$C_{38}H_{38}BaCo_2N_4O_{14}$	$C_{39}H_{39}CaCl_3Co_2N_4O_{14}$
Formula weight	1014.59	1029.92	1052.03
T (K)	293(2)	296(2)	296(2)
Wavelength (Å)	0.71073	0.71073	0.71073
Crystal system	Monoclinic	Triclinic	Triclinic
Space group	$P\ 2_1/n$	P-1	P-1
a (Å)	11.1657(8)	12.6248(5)	12.5212(8)
b (Å)	13.5989(9)	13.3958(6)	13.1612(10)
c (Å)	28.9628(17)	15.2840(6)	13.3725(8)
α	90.00	110.4800(10)	82.562(2)
β	96.758(7)	101.1890(10)	80.553(2)
γ	90.00	99.6460(10)	86.513(2)
Volume (Å^3)	4367.2(5)	2296.13(17)	2153.8(3)
Z	4	2	2
D_c (g•cm^{-3})	1.543	1.490	1.622
θ range for data collection(°)	3.60 to 70.25	2.419 to 25.025	2.318 to 25.397
F(000)	2088	1032	1076
$h/k/l$(min, max)	−13,13/−11,16/−35,32	−14,15/−15,12/−17,18	−15,15/−10,15/−16,16
Crystal size (mm)	0.28 × 0.24 × 0.22	0.25 × 0.16 × 0.14	0.27 × 0.25 × 0.22
Reflections collected	16991/8104 [$R_{int} = 0.0574$]	16502/8031 [$R_{int} = 0.0258$]	16163/7859 [$R_{int} = 0.0317$]
Independent reflection	8104	8031	7859
Completeness to 26.32 (%)	99.82	99.20	99.30
Data/restraints/parameters	8104/0/623	8031/0/536	7859/1/566
Final R indices [$I > 2\sigma(I)$][a]	$R_1 = 0.0553$, $wR_2 = 0.1192$	$R_1 = 0.0306$, $wR_2 = 0.0751$	$R_1 = 0.0530$, $wR_2 = 0.1290$
R indices (all data)[b]	$R_1 = 0.1013$, $wR_2 = 0.1508$	$R_1 = 0.0385$, $wR_2 = 0.0776$	$R_1 = 0.0787$, $wR_2 = 0.1438$
Goodness-of-fit for (F^2)[c]	1.015	1.063	1.025

[a] $R_1 = \Sigma||F_o| - |F_c||/\Sigma|F_o|$;

[b] $wR_2 = [\Sigma w(F_o^2 - F_c^2)^2/\Sigma w(F_o^2)^2]^{1/2}$, $w = [\sigma^2(F_o^2) + (0.0784P)^2 + 1.3233P]^{-1}$, where $P = (F_o^2 + 2F_c^2)/3$; c. GOF = $[\Sigma w(F_o^2 - F_c^2)^2/n_{obs} - n_{param})]^{1/2}$;

an evidence of coordination between ligand H_4L and the added Co(II) ions. The spectroscopic titration clearly indicates the formation of a 1:3 homo-trinuclear complex **1** (Figure 9).

In the UV–vis titration experiments of complex **2**, the spectroscopic titration clearly shows the reaction stoichiometry ratio to be 1:1 (Figure 9). The spectrum of L-Co(II) complex shows a absorption peak at 374 nm, however, upon addition of 1 equiv of Ba(II) ions, the peak only experienced a blue shift of *ca*. 6 nm with maximum peak at 368 nm. For complex **3**, the absorption peak of L-Co(II) complex at 374 nm exhibits a blue shift of *ca*. 8 nm when addition of 1 equiv of Ca(II) ions.

2.4 | Catechol oxidase studies and kinetics

3,5-Di-*tert*-butylcatechol (3,5-$DTBCH_2$) is widely used as the model substrate in most of the catecholase activity studies, the reason being that its oxidized product, 3,5-di-*tert*-butylquinone (3,5-DTBQ), has a characteristic absorption band at around 405 nm (ε = 1900 $M^{-1}\cdot cm^{-1}$) in MeCN.[47,48] Catechol oxidase activity and kinetic parameters could be determined by monitoring the absorption maximum of the quinone. The catechol oxidation reaction of complex **1** with 3,5-$DTBCH_2$ was evaluated by means of UV–vis spectroscopy at room temperature. Solution of complex **1** was treated with 100 equivalents of 3,5-$DTBCH_2$ under aerobic conditions, with the mixture measured at 5 min interval. Figure 10 shows the observed changes in the UV–vis spectra of complex **1** upon addition of 3,5-$DTBCH_2$ (2.5×10^{-3} M) into complex **1** (2.5×10^{-5} M). The spectra of the mixture of complex **1** and 3,5-$DTBCH_2$ were recorded at an interval of 5 min for a total time of 90 min. However, as time progresses, the catalytic process slow down over time, probably due to the influence of the accumulated quinone product (3,5-DTBQ).[49] It is worth noting that hetero-trinuclear complexes **2** and **3** also show catechol oxidase activities (Figure S4).

Kinetic studies of the catecholase activity of complex **1** were performed in order to understand its degree of efficiency. A solution of complex **1** in MeCN was treated with a 100-fold concentrated solution of 3,5-$DTBCH_2$. A 40 μll solution of 3,5-$DTBCH_2$ with a constant concentration of 2.5×10^{-2} M was added to solution of complex **1** (3 ml) so as to achieve the ultimate concentration of complex **1** as 2.5×10^{-5} M. The concentration of 3,5-$DTBCH_2$ ranges from 2.5×10^{-3} to 2.5×10^{-2} M. In order to obtain the initial rate substrate to catalyst ratio, the change in absorbance-time graph was plotted (Abs. = 405 nm) (Figure 11). The rate versus concentration of substrate data were analyzed

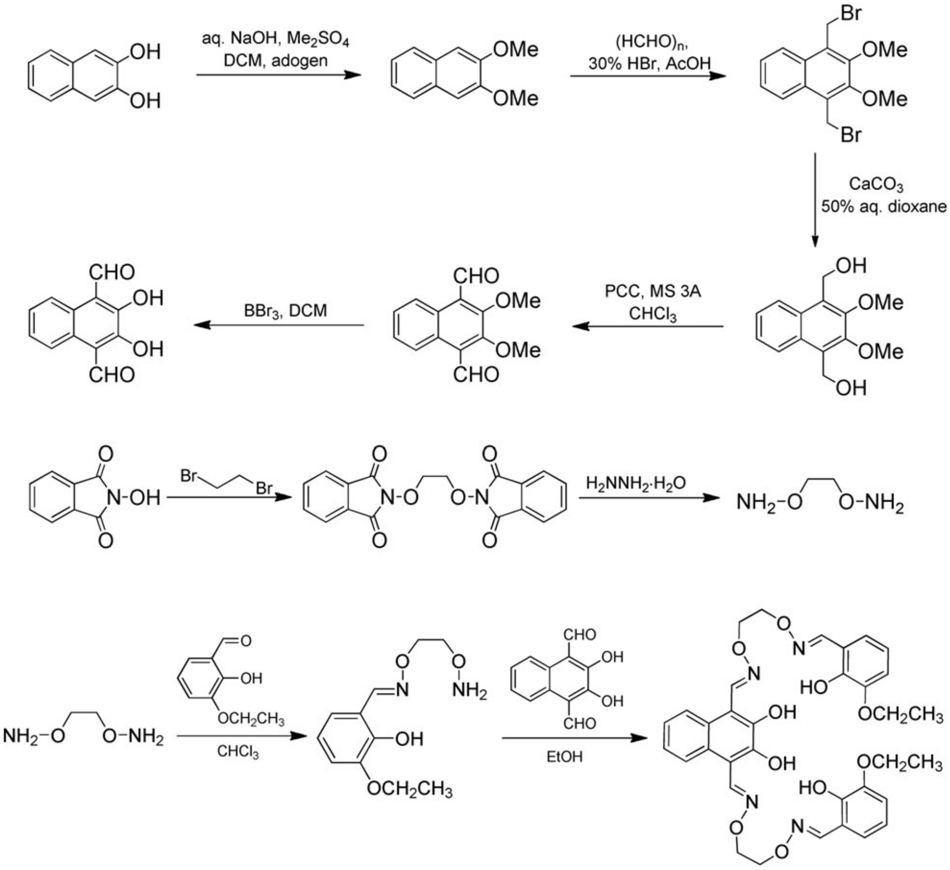

SCHEME 2 Synthesis route to bis(Salamo)-type ligand H_4L

on the basis of Michaelis–Menten enzymatic kinetics to get the double reciprocal Lineweaver-Burk plot as well as the values of the various kinetic parameters V_{max}, K_M and K_{cat} (Figure 12). The turnover number (K_{cat}) is found to be 55.7 h^{-1}.

2.4.1 | Mechanism of catecholase activity

To obtain a mechanistic inference of the catecholase activity and to get an idea about the complex-substrate intermediate, we recorded the ESI-MS spectrum of a 1:100 mixture of complex **1** and 3,5-DTBCH_2. The signal at m/z = 243 (Figure S7; Supporting information) can be assigned to the sodium aggregate of quinone $[3,5\text{-DTBQ-Na}]^+$. The ligand $[H_4L\text{-H}]^+$ exhibits a peak at m/z = 661 (Figure S7; Supporting information). The peak at m/z = 683 (Figure S5; Supporting information) denotes the sodium aggregate of ligand $[H_4L\text{-Na}]^+$. The peak at m/z = 1077 (Figure S6; Supporting information) denotes the formation of the intermediate $[Co_3(L)(3,5\text{-DTBC})\text{-Na}]^+$ (Scheme 1).

The ESI-MS spectrum of a 1:100 mixture of complex **2** and 3,5-DTBCH_2 was recorded. The signal at m/z = 243 (Figure S9; Supporting information) can be assigned to the sodium aggregate of quinone $[3,5\text{-DTBQ-Na}]^+$. The peak at m/z = 683 (Figure S9; Supporting information) denotes the sodium aggregate of ligand $[H_4L\text{-Na}]^+$. The signal at m/z = 1088 (Figure S10; Supporting information) denotes the intermediate $[Co_2Ba(L^{\text{-OEt}})(3,5\text{-DTBQ})]^+$.

We also recorded the ESI-MS spectrum of a 1:100 mixture of complex **3** and 3,5-DTBCH_2. The signals at m/z = 243, 661 and 683 (Figure S13, S11 and S12; Supporting information) can be assigned to the $[3,5\text{-DTBQ-Na}]^+$, $[H_4L\text{-H}]^+$ and $[H_4L\text{-Na}]^+$, respectively. The peak at m/z = 1073 (Figure S12; Supporting information) denotes the formation of the intermediate $[Co_2Ca(L)(3,5\text{-DTBC})\text{-K}]^+$.

3 | CONCLUSIONS

In this paper, we have described the syntheses of a series of homo- and hetero- trinuclear cobalt(II) complexes based on an acyclic symmetrical bis(Salamo)-type tetraoxime ligand H_4L. Interestingly, in addition to Co(II) ions, we have introduced alkaline earth metal ions into the complexes, and finally obtained hetero-trinuclear complexes **2** and **3** resulting in different properties of the complexes. We also studied the reaction stoichiometry ratio through UV–vis titration experiments. According to the data obtained from the catechol oxidase activity and kinetics, we have concluded that the homo-trinuclear complex **1** has a good catechol oxidase activity and kinetics, with the kinetic constant of 55.7 h^{-1} determined by Michaelis–Menten equation.

4 | EXPERIMENTAL

4.1 | General details

3-Ethoxysalicylaldehyde was purchased from Tokyo Chemical Industry and was used without further purification. Other reagents and solvents were of analytical grade supplied by Tianjin Chemical Reagent Factory. Elemental analyses were performed by using a GmbH VarioEL V3.00 automatic elemental analysis instrument. FT-IR spectra were recorded on a VERTEX70 FT-IR spectrophotometer, with samples prepared as KBr (400–4000 cm^{-1}) pellets. UV–vis absorption spectra were recorded on a Hitachi U-3900H spectrometer. ^{1}H NMR spectra were determined by German Bruker AVANCE DRX-400 spectroscopy. FTICR-MS spectra were obtained on a Bruker Daltonics APEX-II 47e spectrometer. The powder X-ray diffractions (PXRD) were recorded by a RIGAKU-DMAX2500 X-ray diffractometer using Cu Kα radiation (λ = 0.154 nm) at a scanning rate of 5 /min for 2θ ranging from 5 to 50.

4.2 | X-ray crystallography

The crystallographic data for complexes **1**, **2** and **3** are summarized in Table 1. X-ray single-crystal diffraction data were collected on a graphite monochromated Mo-K_α radiation (λ = 0.71073 Å) at 293(2), 296(2) and 296(2) K for complexes **1**, **2** and **3**, respectively. Complexes **1**, **2** and **3** crystallize in the monoclinic, triclinic and triclinic with space groups $P2_1/n$, P-1 and P-1, respectively. The structures were solved by using the program SHELXS-97 and Fourier difference techniques, and refined by full-matrix least-squares method on F^2 using SHELXL-97.[50] And the H atoms were included at the calculated positions and constrained to ride on their parent atoms.

4.3 | Syntheses of H_4L and its complexes

4.3.1 | Syntheses of H_4L.

The bis(Salamo)-type tetraoxime ligand (H_4L) was obtained by the reaction of 2,3-dihydroxynaphthalene-1,4-dicarbaldehyde with 3-ethoxysalicylaldehyde. The synthetic route to H_4L is shown in Scheme 2. The 2,3-dihydroxynaphthalene-1,4-dicarbaldehyde was synthesized by the standard method according to the literature.[21,22,51] The ^{1}H NMR spectrum of the ligand obtained shows clearly that it was highly symmetrical. Yield: 43.1%. m.p: 161–162 °C. Anal. calc. For $C_{34}H_{36}N_4O_{10}$ (%): C, 61.81; H, 5.49; N, 8.48. Found (%): C, 61.86; H, 5.42; N, 8.39. Selected IR bands (KBr pellet, cm^{-1}): 3391 (s), 2978 (w), 1605 (m), 1470 (s), 1257 (s), 1064(m). ^{1}H NMR: δ 1.45(s, 6H), 4.08(s, 4H), 4.58(s, 8H), 6.83(s, 6H), 7.41–7.96(dd, 4H), 8.31–9.14

(d, 4H), 9.72–11.0(d, 4H). UV–vis [in chloroform/methanol (3:2)], λ_{max} (nm) [2.5×10^{-5} M]: 263, 341, 359, 378.

4.3.2 | Syntheses of $[Co_3(L)(OAc)_2(CH_3CH_2OH)(H_2O)]$ (1)

A solution of $Co(OAc)_2{\cdot}4H_2O$ (7.88 mg, 0.03 mmol) in methanol (3 ml) was added dropwisely to a stirring solution of H_4L (6.32 mg, 0.01 mmol) in chloroform (3 ml). The dark red solution was filtered and allowed to stay in open air for slow evaporation. After 3 days, the clear dark brown block-shaped crystals of complex **1** were collected, washed with ethanol and n-hexane, and dried in a vacuum drying oven. Yield: 5.08 mg, 52.2%. Anal. calc. For $C_{40}H_{45}Co_3N_4O_{16}$ (%): C, 47.35; H, 4.47; N, 5.52; Co, 17.43. found (%): C, 47.51; H, 4.39; N, 5.67; Co, 17.35. Selected IR bands (KBr pellet, cm^{-1}): 3429 (m), 2978 (w), 1592 (m), 1457 (s), 1205 (s), 1083 (m). UV–vis [in chloroform/methanol (3:2)], λ_{max} (nm) [2.5×10^{-5} M]: 342, 358 and 378.

4.3.3 | Syntheses of $[Co_2Ba(L)(OAc)_2]$ (2)

Complex **2** was prepared by the addition of $Co(OAc)_2{\cdot}4H_2O$ (7.86 mg,0.03 mmol) and $Ba(OAc)_2$ (2.77 mg 0.01 mmol) in a mixed solution of methanol (3 ml) and water (0.5 mL). To the resulting solution was added dropwisely to a stirring solution of H_4L (6.68 mg, 0.01 mmol) in chloroform (3 ml). The deep red solution was filtered and kept for a week in open air for slow evaporation, the dark brown crystals suitable for X-ray analysis were obtained, and finally dried in a vacuum drying oven. Yield: 5.25 mg (51.0%).Anal. calc. For $C_{38}H_{38}BaCo_2N_4O_{14}$(%): C, 44.31; H, 3.72;N, 5.44; Ba, 13.33; Co, 11.44. Found (%): C, 44.68; H, 3.67; N, 5.21; Ba, 13.15; Co, 11.48. Selected IR bands (KBr pellet, cm^{-1}): 2933 (w), 1585 (m), 1457 (s), 1210 (s), 1057 (m). UV–vis [in chloroform/methanol (3:2)], λ_{max} (nm) [2.5×10^{-5} M]: 282, 370 and 418.

4.3.4 | Syntheses of $[Co_2Ca(L)(OAc)_2]{\cdot}CHCl_3$ (3)

A mixed solution of $Co(OAc)_2{\cdot}4H_2O$ (7.62 mg, 0.03 mmol) and $Ca(OAc)_2{\cdot}H_2O$(1.92 mg, 0.01 mmol) in ethanol solution (3 ml) was added dropwisely to a stirred solution of H_4L (7.06 mg, 0.01 mmol) in chloroform (3 ml). The resulting wine red solution was filtered and brown crystals suitable for X-ray analysis were obtained after several days, and then washed and dried just like **1** and **2**. Yield: 6.42 mg (61.0%). Anal. calc. For $C_{39}H_{39}CaCl_3Co_2N_4O_{14}$ (%): C, 44.52; H, 3.74; N, 5.33; Ca, 3.81; Co, 11.20. Found (%): C, 45.38; H, 3.67; N, 5.21; Ca, 3.77; Co, 11.26. Selected IR bands (KBr pellet, cm^{-1}): 2984 (w), 1590 (s), 1464 (m), 1206 (s), 1090 (m). UV–vis [in chloroform/methanol (3:2)], λ_{max} (nm) [2.5×10^{-5} M]: 244, 273 and 367.

In order to confirm the crystal structures of complexes **1**, **2** and **3**, the PXRD experiments are carried out in this paper (as shown in Figure S14-S16). By contrast, the results of the experiment patterns and the simulated ones are in good agreements, which confirms the purity of those complexes. Therefore, the samples are pure enough for the study of their properties.

ACKNOWLEDGMENTS

This work was supported by the National Natural Science Foundation of China (21361015), which is gratefully acknowledged.

REFERENCES

[1] R. M. Haak, A. Decortes, E. C. Escudero-Adán, M. M. Belmonte, E. Martin, J. B. Buchholz, A. W. Kleij, *Inorg. Chem.* **2011**, *50*, 7934.

[2] H. L. Wu, G. L. Pan, Y. C. Bai, Y. H. Zhang, H. Wang, F. R. Shi, X. L. Wang, *J. Photochem. Photobiol. B* **2014**, *135*, 33.

[3] H. L. Wu, Y. C. Bai, Y. H. Zhang, Z. Li, M. C. Wu, C. Y. Chen, J. W. Zhang, *J. Coord. Chem.* **2014**, *67*, 3054.

[4] C. Y. Chen, J. W. Zhang, Y. H. Zhang, Z. H. Yang, H. L. Wu, G. L. Pana, Y. C. Bai, *J. Coord. Chem.* **2015**, *68*, 1054.

[5] H. L. Wu, C. P. Wang, F. Wang, H. P. Peng, H. Zhang, Y. C. Bai, *J. Chin. Chem. Soc.* **2015**, *62*, 1028.

[6] H. L. Wu, Y. C. Bai, Y. H. Zhang, G. L. Pan, J. Kong, F. Shi, X. L. Wang, *Z. Anorg. Allg. Chem.* **2014**, *640*, 2062.

[7] S. Kal, A. S. Filatov, P. H. Dinolfo, *Inorg. Chem.* **2014**, *53*, 7137.

[8] P. G. Lacroix, *Eur. J. Inorg. Chem.* **2001**, *2001*, 339.

[9] H. L. C. Feltham, R. Clérac, L. Ungur, L. F. Chibotaru, A. K. Powell, S. Brooker, *Inorg. Chem.* **2013**, *52*, 3236.

[10] S. T. Zhang, T. R. Li, B. D. Wang, Z. Y. Yang, J. Liu, Z. Y. Wang, W. K. Dong, *Dalton Trans.* **2014**, *43*, 2713.

[11] X. Q. Song, P. P. Liu, Y. A. Liu, J. J. Zhou, X. L. Wang, *Dalton Trans.* **2016**, *45*, 8154.

[12] C. E. Burrow, T. J. Burchell, P. H. Lin, F. Habib, W. Wernsdorfer, R. Clérac, M. Murugesu, *Inorg. Chem.* **2009**, *48*, 8051.

[13] X. Q. Song, Y. K. Lei, X. R. Wang, M. M. Zhao, Y. Q. Peng, G. Q. Cheng, *J. Solid State Chem.* **2014**, *218*, 202.

[14] T. Z. Yu, K. Zhang, Y. L. Zhao, C. H. Yang, H. Zhang, L. Qian, D. W. Fan, W. K. Dong, L. L. Chen, Y. Q. Qiu, *Inorg. Chim. Acta* **2008**, *361*, 233.

[15] T. Z. Yu, K. Zhang, Y. L. Zhao, C. H. Yang, H. Zhang, D. W. Fan, W. K. Dong, *Inorg. Chem. Commun.* **2007**, *10*, 401.

[16] M. Tsunoda, M. Fleischmann, J. S. Jones, N. Bhuvanesh, M. Scheer, F. P. Gabbaï, *Dalton Trans.* **2016**, *45*, 5045.

[17] P. P. Liu, L. Sheng, X. Q. Song, W. Y. Xu, Y. A. Liu, *Inorg. Chim. Acta* **2015**, *434*, 252.

[18] X. Q. Song, Y. J. Peng, G. Q. Chen, X. R. Wang, P. P. Liu, W. Y. Xu, *Inorg. Chim. Acta* **2015**, *427*, 13.

[19] I. Nemec, R. Herchel, T. Šilha, Z. Trávníček, *Dalton Trans.* **2014**, *43*, 15602.

[20] X. Q. Song, P. P. Liu, Z. R. Xiao, X. Li, Y. A. Liu, *Inorg. Chim. Acta* **2015**, *438*, 232.

[21] S. Akine, T. Tadokoro, T. Nabeshima, *Inorg. Chem.* **2012**, *51*, 11478.

[22] S. Akine, S. Sairenji, T. Taniguchi, T. Nabeshima, *J. Am. Chem. Soc.* **2013**, *135*, 12948.

[23] S. Akine, W. K. Dong, T. Nabeshima, *Inorg. Chem.* **2006**, *45*, 4677.

[24] S. Akine, T. Nabeshima, *Dalton Trans.* **2009**, *47*, 10395.

[25] S. Akine, *J. Inclusion Phenom. Macrocyclic Chem.* **2012**, *72*, 25.

[26] S. Akine, T. Taniguchi, T. Nabeshima, *Inorg. Chem.* **2008**, *47*, 3255.

[27] H. L. Wu, G. L. Pan, Y. C. Bai, H. Wang, J. Kong, F. R. Shi, Y. H. Zhang, X. L. Wang, *J. Chem. Res.* **2014**, *38*, 211.

[28] H. L. Wu, G. L. Pan, Y. C. Bai, H. Wang, J. Kong, F. R. Shi, Y. H. Zhang, X. L. Wang, *J. Coord. Chem.* **2013**, *66*, 2634.

[29] Y. X. Sun, W. K. Dong, L. Wang, L. Zhao, Y. H. Yang, *Chin. J. Inorg. Chem.* **2009**, *25*, 1478.

[30] T. Z. Yu, W. M. Su, W. L. Li, Z. R. Hong, R. N. Hua, M. T. Li, B. Chu, B. Li, Z. Q. Zhang, Z. Hu, *Inorg. Chim. Acta* **2006**, *359*, 2246.

[31] W. K. Dong, J. C. Ma, L. C. Zhu, Y. Zhang, *New J. Chem.* **2016**, *40*, 6998.

[32] W. K. Dong, J. C. Ma, L. C. Zhu, Y. X. Sun, S. F. Akogun, Y. Zhang, *Cryst. Growth Des.* **2016**, *16*, 6903.

[33] W. K. Dong, X. L. Li, L. Wang, Y. Zhang, Y. J. Ding, *Sensors Actuators B Chem.* **2016**, *229*, 370.

[34] W. K. Dong, S. F. Akogun, Y. Zhang, Y. X. Sun, X. Y. Dong, *Sensors Actuators B Chem.* **2017**, *238*, 723.

[35] W. K. Dong, J. C. Ma, Y. J. Dong, L. C. Zhu, Y. Zhang, *Polyhedron* **2016**, *115*, 228.

[36] W. K. Dong, J. Zhang, Y. Zhang, N. Li, *Inorg. Chim. Acta* **2016**, *444*, 95.

[37] W. K. Dong, P. F. Lan, W. M. Zhu, Y. Zhang, *J. Coord. Chem.* **2016**, *69*, 1272.

[38] W. K. Dong, J. T. Zhang, Y. J. Dong, Y. Zhang, Z. K. Wang, *Z. Anorg. Allg. Chem.* **2016**, *642*, 189.

[39] Y. X. Sun, L. Wang, X. Y. Dong, Z. L. Ren, W. S. Meng, *Synth. React. Inorg., Met.-Org., Nano-Met. Chem.* **2013**, *43*, 599.

[40] Y. X. Sun, L. Xu, T. H. Zhao, S. H. Liu, G. H. Liu, X. T. Dong, *Synth. React. Inorg., Met.-Org., Nano-Met. Chem.* **2013**, *43*, 509.

[41] X. Y. Dong, Y. X. Sun, L. Wang, L. Li, *J. Chem. Res.* **2012**, 387.

[42] L. Zhao, L. Wang, Y. X. Sun, W. K. Dong, X. L. Tang, X. H. Gao, *Synth. React. Inorg., Met.-Org., Nano-Met. Chem.* **2012**, *42*, 1303.

[43] L. Zhao, X. T. Dang, Q. Chen, J. X. Zhao, L. Wang, *Synth. React. Inorg., Met.-Org., Nano-Met. Chem.* **2013**, *43*, 1241.

[44] P. Wang, L. Zhao, *Spectrochim Acta Part A* **2015**, *135*, 342.

[45] M. C. Heffern, N. Yamamoto, R. J. Holbrook, A. L. Eckermann, T. J. Meade, *Curr. Opin. Chem. Biol.* **2013**, *17*, 189.

[46] A. W. Addison, T. N. Rao, J. Reedijk, J. Rijn, G. C. Verschoor, *Dalton Trans.* **1984**, *14*, 1349.

[47] R. Sanyal, P. Kundu, E. Rychagova, G. Zhigulin, S. Ketkov, B. Ghosh, S. K. Chattopadhyay, E. Zangrando, D. Das, *New J. Chem.* **2016**, *40*, 6623.

[48] A. Szorcsik, F. Matyuska, A. Benyei, N. V. Nagy, R. K. Szilagyi, T. Gajda, *Dalton Trans.* **2016**, *45*, 14998.

[49] I. A. Koval, K. Sehmeczi, C. Belle, C. Philouze, E. SaintAman, I. Gautier-Luneau, A. M. Schuitema, M. Vliet, P. Gamez, O. Roubeau, M. Luken, B. Krebs, M. Lutz, A. L. Spek, J. L. Pierre, J. Reedijk, *Chem. – Eur. J.* **2006**, *12*, 6138.

[50] G. M. Sheldrick, *SHELXS-97 and SHELXL-97,* Fortran Programs for Crystal Structure Solution and Refinement, University of Gottingen, Gottingen **1997**.

[51] H. A. Tran, J. Collins, P. E. Georghiou, *New J. Chem.* **2008**, *32*, 1175.

SUPPORTING INFORMATION

Additional Supporting Information may be found online in the supporting information tab for this article.
CCDC Nos: 1522113–1522115 contain supplementary crystallographic data for complexes **3**, **1** and **2**. These data can be obtained free of charge from the Cambridge Crystallographic Data Centre via www.ccdc.cam.ac.uk/datarequest/cif.

How to cite this article: Li L-H, Dong W-K, Zhang Y, Akogun SF, Xu L. Syntheses, structures and catecholase activities of homo- and hetero-trinuclear cobalt(II) complexes constructed from an acyclic naphthalenediol-based bis(Salamo)-type ligand. *Appl Organometal Chem*. 2017;e3818. https://doi.org/10.1002/aoc.3818